

MOL #68619

A state-dependent salt-bridge interaction exists across the β/α inter-subunit interface of the GABA_A receptor.

Kurt T. Laha and David A. Wagner

Department of Biological Sciences, Marquette University, Milwaukee, Wisconsin 53201 USA

MOL #68619

Running title: State-dependent salt-bridge interaction

Corresponding Author:

Kurt T. Laha

Department of Biological Sciences,

Marquette University

P.O. Box 1881

Milwaukee, Wisconsin 53201-1881, USA

Phone: (414) 288-5695

Fax: (414) 288-7357

Email: kurt.laha@marquette.edu

Number of text pages:	38
Number of tables:	2
Number of figures:	7
Number of References:	38
Number of words in Abstract:	190
Number of words in Introduction:	563
Number of words in Discussion:	1402

List of non-standard abbreviations:

LGIC = ligand-gated ion channel

SCAM = substituted cysteine accessibility method

MOL #68619

Abstract

The GABA_A receptor is a multi-subunit protein that transduces the binding of a neurotransmitter at an inter-subunit interface into the opening of a central ion channel. The structural components that mediate the steps involved in this action are poorly defined. A large amount of work has focused on clarifying the specific functions and interactions of residues believed to surround the GABA binding pocket. Here we explored two charged residues (β_2 D163 and α_1 R120), which have been suggested by homology models to participate in a salt-bridge interaction. When mutated to alanine, both single mutants, as well as the double mutant, increase EC_{50-GABA}, decrease the GABA binding rate, and accelerate deactivation and GABA unbinding rates. Double-mutant cycle analysis demonstrates that the effects of each alanine mutation on the GABA binding rate were additive and independent. In contrast, a significant coupling energy was found when analyzing deactivation time constants. Using kinetic modeling we further demonstrated that the GABA unbinding rates, in particular, are strongly coupled. These data suggest that β_2 D163 and α_1 R120 form a state-dependent salt-bridge, interacting when GABA is bound to the receptor but not when the receptor is in the unbound state.

MOL #68619

Introduction

The GABA_A receptor is a member of the cys-loop family of ligand gated ion channels (LGICs), which also includes nicotinic acetylcholine, serotonin (5-HT₃), and glycine receptors. The cys-loop LGICs mediate fast synaptic transmission throughout the central and peripheral nervous system as the binding of a neurotransmitter to the extracellular domain of a receptor leads to the opening of an intrinsic ion pore. The GABA_A receptor contains a chloride channel and is the major type of inhibitory neurotransmitter receptor in the mammalian CNS. It is the target of sedatives, anxiolytics, anti-epileptics, and general anesthetics.

The GABA_A receptor, along with all cys-loop LGICs, is a pentameric protein, constructed of homologous subunits. These subunits are arranged pseudo-symmetrically around a central ion-conducting pore. The most abundant complex found in the brain consists of two α_1 , two β_2 , and one γ_2 subunit (Benke et al., 1994; McKernan and Whiting; 1996). It is arranged counter-clockwise as $\beta\alpha\gamma\beta\alpha$ (Baumann et al., 2002). The neurotransmitter γ -aminobutyric acid (GABA) is believed to bind at the extracellular interface of the β and α subunits. This idea is supported by a plethora of studies that have utilized site-directed mutagenesis, photoaffinity labeling, and substituted cysteine accessibility method (SCAM) to identify over 20 amino acids from the α and β subunits that appear to play a role in GABA binding (Kash et al., 2004). Specific roles for a handful of these residues have been proposed. For example, β_2 Y97 may form a cation- π bond with the amino group of GABA (Padgett et al., 2007), but by and large it is unclear whether a given residue implicated in GABA binding directly interacts with GABA, stabilizes the structure of the binding pocket, or is involved in transducing binding into channel gating.

MOL #68619

Homology models (Cromer et al., 2002; Omara et al., 2005) derived from the crystallized structure of the molluscan acetylcholine binding protein (AChBP) (Brejc et al., 2001) have been used to generally position the residues in the binding pocket and can further inform us as to the role of an individual residue. However, interpretations drawn from these models must be experimentally verified. One interpretation drawn from homology models is that an arginine from the α subunit (α_1 R120) forms an inter-subunit salt-bridge with an aspartate from the β subunit (β_2 D163), and that this salt bridge is conserved at every subunit interface (Cromer et al., 2002) (Fig. 1). These two residues are highly conserved among LGIC subunits and experimental evidence for a corresponding salt-bridge interaction has been presented for the γ/β inter-subunit interface of the GABA_A receptor (Goldschen-Ohm et al., 2010). Mutagenesis studies show the GABA concentration-response curve is sensitive to changes at either α_1 R120 or β_2 D163 (Westhansen et al., 1999; Kloda and Czajkowski, 2007; Newell et al., 2004). Also, SCAM studies demonstrated both residues are accessible to modification by sulfhydryl reactive reagents, indicating that they are present at the aqueous surface (Newell et al., 2004; Kloda and Czajkowski, 2007).

We explored this postulated interaction between α_1 R120 and β_2 D163 by characterizing macroscopic parameters ($EC_{50-GABA}$, deactivation, and desensitization) and microscopic parameters (GABA binding and unbinding rates) for alanine mutations at each residue. These results were subjected to double-mutant cycle analysis. Interestingly, mutation of both residues affected the GABA binding rate ($k_{on-GABA}$), independently. However, when analyzing the deactivation time constants or the GABA unbinding rates, the two residues appear to be coupled. These results suggest that α_1 R120 and β_2 D163 form a state-dependent salt-bridge.

MOL #68619

Materials and Methods

cDNA constructs and mutagenesis:

Human α_1 , β_2 , and γ_{2S} subunits inserted into the pcDNA 3.1 vector were used. A β_2 variant (β_{2-GKER}) that has been developed experimentally was used in order to rescue expression with α_1R120A . β_{2-GKER} has four amino acids of β_2 replaced with the aligned residues found on the β_3 subunit, D171G, N173K, T179E, and K180R (Taylor et al., 1999; Bollan et al., 2003). **These residues are located proximal to the cell membrane and are on the non-GABA binding face of the subunit.** This subunit has been shown to assemble more efficiently (Bollan et al., 2003) and we have found no differences in kinetics, $EC_{50-GABA}$, or amplitude between β_2 and β_{2-GKER} containing receptors. For all of the results presented here $\alpha_1\beta_{2-GKER}\gamma_{2S}$ receptors are used as the control. Mutant α_1 and β_2 subunits were created using the QuikChange II site-directed mutagenesis kit (Stratagene, La Jolla, CA), and double stranded sequencing of the entire coding region was conducted in order to verify fidelity.

Cell Culture, Transfection, and Labeling:

Human embryonic kidney (HEK-293) cells were cultured in Minimum Essential Medium Eagle with Earle's salts (Mediatech, Manassas, VA) supplemented with 10% newborn calf serum (Thermo Scientific, Waltham, MA) and Penicillin-Streptomycin-Glutamine (Mediatech) in a 37°C incubator under a 5% CO₂ atmosphere. Cells were plated onto 35 mm dishes coated with poly-L-lysine and were transfected 18-24 hours later using Lipofectamine 2000 (Invitrogen, Carlsbad, CA) and the following amounts of cDNA: 250ng eGFP, 1 μ g of α_1 (wild-type or R120A), 1 μ g β_{2-GKER} (wild type or D163A), and 3 μ g of γ_{2S} . Cells were recorded from 48-96 hours post-transfection.

MOL #68619

Electrophysiology:

All recordings for this study were collected from outside-out patches excised from HEK-293 cells (-60 mV). Recordings were made using borosilicate glass pipettes filled with (in mM): 140 KCl, 10 EGTA, 2 MgATP, 20 phosphocreatine and 10 HEPES, pH 7.3. Rapid solution exchange was accomplished by using a multibarreled flowpipe array (Vitrodynamics, Rockaway, NJ) mounted on a piezoelectric bimorph (Vernitron, Bedford, OH). A computer-controlled constant current source drove the bimorph to move solution interfaces over the patch with 10-90% exchange times of ~200 μ s, as measured by the liquid junction current at the open pipette tip after each experiment. GABA_A receptor agonists and antagonists were dissolved in the perfusion solution, which contains (in mM) 145 NaCl, 2.5 KCl, 2 CaCl₂, 1 MgCl₂, 10 HEPES, 4 mM Glucose, pH 7.4. For extracellular solutions that contained >30 mM GABA, the concentration of NaCl was reduced to 95 mM, and a combination of sucrose and GABA was added to compensate for the reduced osmolarity. The pipette solution was adjusted in conjunction, reducing the KCl concentration to 90 mM, and adding 50 mM K-gluconate to maintain a constant Cl⁻ driving force. GABA and SR-95531 were obtained from Sigma-Aldrich Chemicals, St Louis, Mo. Currents were low-pass filtered at 2-5 kHz with a four-pole Bessel filter, and digitized at a rate no less than twice the filter frequency. Data were collected at 20 kHz using an Axopatch 200B amplifier (Axon Instruments, Foster City, CA) and an ITC-1600 digitizer (InstruTech, Port Washington, NY), controlled by Axograph X software (Axograph Scientific, Sydney, AUS). Macroscopic current ensembles were collected with 15 second intervals between consecutive solution applications. Curve fitting was also performed using Axograph X software.

Deactivation and desensitization phases were fit with bi-exponential functions. For

MOL #68619

deactivation, the time of GABA removal was set to zero, and the region of deactivation was fit with the equation $Y = A_1 \cdot e^{-t/\tau_1} + A_2 \cdot e^{-t/\tau_2}$. For desensitization, the onset of desensitization was set to zero, and region of desensitization was fit with the equation $Y = A_1 \cdot e^{-t/\tau_1} + A_2 \cdot e^{-t/\tau_2} + C$. A weighted time constant (τ_w) was also calculated for each analysis. $\tau_w = (A_1/(A_1 + A_2)) \cdot \tau_1 + (A_2/(A_1 + A_2)) \cdot \tau_2$. Figures of raw data represent ensemble averages of 10-30 traces that have been decimated. In all cases significant differences were tested using one-way ANOVA with a post-hoc Dunnett's test, at a significance level of $p < 0.05$ (Prism 4, GraphPad Software, Inc., San Diego, CA).

Antagonist unbinding experiments:

Outside-out patches were pre-equilibrated in SR-95531 for 750 ms, and then rapidly switched to a solution containing saturating GABA. The evoked current was shaped by the convolution of the time course of antagonist unbinding and the waveform of the control current (evoked with no pre-equilibration in antagonist). Home-written Matlab (Mathworks, Natick, MA) routines were used for the deconvolution of the time course of antagonist unbinding from this evoked current (Jones et al., 2001). The time course of antagonist unbinding was fit with an exponential function, yielding k_{off-SR} and the percentage of receptors occupied by antagonist at equilibrium. The experiment was repeated several times, pre-equilibrating in different concentrations of SR-95531. K_{D-SR} was determined by plotting the antagonist occupancy versus concentration.

Measuring the microscopic binding rate of GABA

The microscopic binding rate of GABA ($k_{on-GABA}$) was measured using "race" experiments (Jones et al., 1998). In a race experiment, agonist (having an *unknown* binding

MOL #68619

rate) is co-applied with an antagonist which has a previously determined binding rate (k_{on-ant} , see "Antagonist Unbinding Experiments" above). The amplitude of the current evoked by co-application of agonist and antagonist is compared to the amplitude of current evoked by agonist alone, and this ratio ($I_{ag-ant}/I_{ag-only}$) is called I_{race} . I_{race} depends only on the relative concentrations and binding rates of agonist and antagonist. The only unknown is the agonist binding rate, $k_{on-agonist}$, which can be solved for using the following equation:

$$k_{on-agonist} = ([antagonist] \cdot k_{on-ant}) / ([agonist] \cdot (1/I_{race} - 1)).$$

Mutant cycle analysis:

Mutant cycle analysis was performed on EC_{50} values, deactivation rates, and binding rates.

$\Delta\Delta G^{\circ}$ was calculated as $RT \ln (k_{mutant}/k_{wild-type})$, where R is the ideal gas constant (1.987 calories/mole) and T is the absolute temperature (296 K). Although EC_{50} and deactivation rates do not provide true kinetic rate constants, comparison of macroscopic parameters have been previously utilized to support side chain interactions and establish coupling coefficients (Kash et al., 2003; Price et al., 2007; Gleitsman et al., 2008). If two mutations have independent effects

$\Delta\Delta G^{\circ}_{(3)} = \Delta\Delta G^{\circ}_{(1)} + \Delta\Delta G^{\circ}_{(2)}$. For our evaluation we set a coupling energy [$\Delta\Delta G^{\circ}_{coupling} = (\Delta\Delta G^{\circ}_{(1)} + \Delta\Delta G^{\circ}_{(2)}) - \Delta\Delta G^{\circ}_{(3)}$] of |0.5| kcal/mol as the cut off for non-additivity.

MOL #68619

Nonstationary Variance analysis:

Nonstationary variance analysis (Sigworth, 1980) was performed on responses to repeated 3 ms pulses of saturating GABA. As previously described (Goldschen-Ohm, et al., 2010; Wagner et al., 2004) Mean current (I) and variance (σ^2) of the repeated pulses were calculated at each time point, mean current was divided into 100 equally sized bins, and the variances in each bin were averaged. The binned variance was plotted versus current and fit with the equation: $\sigma^2 = iI - I^2N^{-1}$, where i is the single channel current, and N is the number of channels. Conductance was calculated by dividing I by the holding potential of -60 mv. Variance resulting from slow drift (i.e., rundown or run-up) was corrected by local linear fitting of the drift, calculating the variance due to this trend at each point, and subtracting the drift variance (scaled by the square current amplitude) from the total variance before fitting. This method yields accurate estimates of i and N when tested on simulated data with drift (Wagner et al., 2004).

Kinetic Modeling:

Kinetic modeling was performed with home-written software using the Q-matrix method (Colquhoun and Hawkes, 1995a,b). We utilized a simplified model of GABA_A receptor behavior (Fig. 6) that has previously been described (Jones et al., 1998; Wagner et al., 2004, Goldschen-Ohm et al., 2010). Although we considered more complex variations of this model, which included additional desensitized and open states, the simplified model was equally suitable to recapitulate our data. During optimization the rate constant k_{on} and P_{o-max} were constrained to the value obtained from experiments in this study; all other parameters were initially set to values reported by Goldschen-Ohm et al. (2010) and were unconstrained. Current responses from 3 ms and 500 ms pulses of saturating GABA were simultaneously fit for each

MOL #68619

patch. Following initial optimization, only k_{off} , r_1 , d_2 , r_2 , and p were left unconstrained; and fits were repeated. Optimization used a simplex algorithm to minimize the amplitude-weighted sum of squared errors between actual and simulated currents. In all cases, significant differences in transition rates were tested using a two-tailed unpaired Student's t test at a significance level of $p < 0.05$ (Prism 4).

MOL #68619

Results

In homology models β_2 D163 and α_1 R120 are juxtaposed across the “top” of the GABA binding pocket. In order to further explore the roles of these residues in receptor function, and to determine if they functionally interact, we replaced each wild type side chain with the methyl group of alanine. Alanine replacement serves to remove electrostatic or hydrogen bonding interactions inherent to the wild type side chains, and minimizes potentially confounding interactions from the introduced side chain. Receptors containing the α_1 R120A mutation, the β_2 D163A mutation, or both mutations were characterized.

β_2 -GKER rescues α_1 R120A expression and γ_2 rescues β_2 D163A expression

HEK 293 cells transfected with wild-type β_2 and α_1 R120A display neither GABA-evoked (100 mM) nor propofol-evoked (300 μ M) current. The propofol binding site is distinct from the GABA binding site where α_1 R120 is located. Therefore it is likely that the α_1 R120A mutation negatively affects **functional expression** of receptors in HEK 293 cells. In order to rescue **functional expression**, we utilized the β_2 -GKER construct. β_2 -GKER contains four point-mutations where a given residue is replaced with its counterpart from the β_3 subunit. This construct has been shown to rescue expression of another binding site mutant, α_1 R67A, (Bollan et al., 2003) and has subsequently been used in our lab to restore **functional expression** to several other mutant constructs (unpublished results).

Transfections with wild type α_1 and β_2 D163A also failed to display GABA or propofol evoked currents. In an attempt to rescue expression, the β_2 D163A mutation was recreated in the β_2 -GKER background, but this construct failed to give current. Ultimately, co-transfection with the γ_2

MOL #68619

subunit was necessary to obtain robust GABA-evoked currents. To ensure adequate expression and to control for any influence of the γ_2 subunit, we performed this study using cells transfected with $\alpha_1\beta_{2\text{-GKER}}\gamma_2$, $\alpha_1\beta_{2\text{-GKER}}\text{D163A}\gamma_2$, $\alpha_1\text{R120A}\beta_{2\text{-GKER}}\gamma_2$, or $\alpha_1\text{R120A}\beta_{2\text{-GKER}}\text{D163A}\gamma_2$, which shall be referred to from here on as wild-type, D163A, R120A, or R120A/D163A respectively.

The sensitivity of this region to mutations was additionally observed during our attempts to express charge reversal mutants of each residue (D163R and R120D), alone or in concert as a charge swap. Transfection with either charge reversal or the swap failed to express functional receptors **when using the $\beta_{2\text{-GKER}}$ construct and the γ_2 subunit.**

Double-mutant cycle analysis of D163A and R120A using $\text{EC}_{50\text{-GABA}}$ yields a weak coupling energy

The primary goal of this study was to determine whether $\beta_2\text{D163}$ and $\alpha_1\text{R120}$ participate in an inter-subunit salt-bridge. A tool that can be used to this end is the method of double-mutant cycle analysis, which quantifies the coupling energy between two mutated residues and clarifies the likelihood of two residues interacting (Horovitz, 1996). One parameter that has been commonly used for double-mutant cycle analysis in the study of LGICs is the apparent affinity for ligand, or EC_{50} (Kash et al., 2003; Price et al., 2007; Gleitsman et al., 2008). Therefore, the effects of the D163A and R120A mutations were initially characterized by determining the peak current $\text{EC}_{50\text{-GABA}}$ value through concentration-response experiments. The D163A mutation caused a 2.4-fold increase in $\text{EC}_{50\text{-GABA}}$ (155 μM) compared to the wild-type (65 μM), whereas the R120A mutation had a much larger effect on $\text{EC}_{50\text{-GABA}}$ causing a 14-fold shift to 900 μM .

MOL #68619

Receptors containing both mutations displayed a 25-fold increase in $EC_{50-GABA}$ (1600 μ M) (Fig. 2A).

EC_{50} values were input into a mutant cycle to obtain a coupling energy of 0.2 kcal/mol (Fig. 2B, Table 2). If β_2 D163 and α_1 R120 are functionally independent with respect to $EC_{50-GABA}$, we would expect the coupling energy to be 0 kcal/mol. Any value that deviates from zero may indicate coupling, but typically a more stringent criterion (*i.e.* a coupling energy of at least |0.5| kcal/mol) is utilized to identify direct interactions between two side chains.

Although studies of LGICs commonly use EC_{50} values to derive thermodynamic energies, these results can be confounded by the complex nature of the EC_{50} value, which depends on multiple microscopic processes that underlie both ligand affinity and channel gating (Colquhoun, 1998; Gleitsman et al., 2008). Therefore, coupling energies calculated from EC_{50} values may be skewed, particularly when exploring interactions that influence multiple parameters or exist only in certain receptor states. The significance of the weak coupling energy found here is unclear, and we cannot confirm or exclude an interaction between β_2 D163 and α_1 R120 with this evidence.

D163A and R120A independently reduce the GABA binding rate

Since analysis of $EC_{50-GABA}$ was indeterminate, we directly measured the microscopic binding rates for GABA for each construct using race experiments, as previously described by Jones et al. (2001). Briefly, the first step in this process is to directly measure the binding rate for a competitive antagonist, in this case SR-95531. Once the binding rate for SR-95531 (k_{on-SR}) is determined, the binding rate of the agonist, GABA, can be measured by performing an

MOL #68619

experiment in which GABA and SR-95531 are co-applied. The resulting current is compared to the current evoked by an application of GABA alone. The extent to which the peak current is reduced by the presence of antagonist depends on the relative binding rates of the two compounds. Since the binding rate of SR-95531 has been determined, the binding rate of GABA ($k_{on-GABA}$) can be calculated.

We characterized the binding kinetics of the competitive antagonist SR-95531 for each receptor type. Antagonist unbinding experiments were employed as previously described (Jones et al., 2001), and we measured the dissociation constant (K_{D-SR}) and microscopic unbinding rate (k_{off-SR}) for each receptor type (Supplemental Fig. 1). Each mutant construct causes a small, albeit significant, ($\approx 30\%$) reduction in k_{off-SR} , but there are no measurable changes in K_{D-SR} (Table 1). k_{on-SR} , which was determined using the equation $k_{on-SR} = k_{off-SR}/K_{D-SR}$, was also not significantly affected by any of the mutations.

Figure 3A depicts the results of the race experiment. The ratio of the peak response of co-application to the peak response to a control application of GABA alone is the result of the relative binding rates and concentrations of GABA and SR-95531. Using this ratio, termed I_{race} , the GABA binding rate can be computed as $k_{on-GABA} = [SR95531] k_{on-SR}/([GABA](1/I_{race} - 1))$ (Jones et al., 1998). Application of 3 mM GABA and 300 μ M SR-95531 gave an I_{race} ratio of 0.41 ± 0.04 for the wild-type receptor, while for the same concentrations I_{race} was reduced to 0.27 ± 0.01 for D163A, indicating a slower binding rate for GABA. R120A and R120A/D163A receptors required a ten-fold increase in the concentration of GABA (30 mM) co-applied with 300 μ M SR-95531 to obtain I_{race} values of 0.37 ± 0.03 and 0.31 ± 0.01 respectively, indicating

MOL #68619

even greater reductions in the GABA binding rate than seen for D163A receptors. Indeed, when these I_{race} values are used to calculate $k_{\text{on-GABA}}$ all of the mutants display significantly reduced GABA binding rates (wild-type: $7.4 \pm 0.4 \times 10^6 \text{ M}^{-1}\text{s}^{-1}$; D163A: $4.3 \pm 0.5 \times 10^6 \text{ M}^{-1}\text{s}^{-1}$; R120A: $8.3 \pm 0.8 \times 10^5 \text{ M}^{-1}\text{s}^{-1}$; R120A/D163A: $5.0 \pm 0.3 \times 10^5 \text{ M}^{-1}\text{s}^{-1}$).

When these numbers are subjected to double-mutant cycle analysis the resulting coupling energy is effectively nil (-0.03 kcal/mol) (Table 2). Therefore, the mutations R120A and D163A demonstrate additive effects on the GABA binding rate, strongly indicative of an independent relationship. During the binding process, a salt-bridge between these residues is either irrelevant or non-existent.

D163A and R120A accelerate the deactivation phase and display significant coupling

Each mutation causes significant changes in EC_{50} and the GABA binding rate; therefore, it is evident that these residues are important for normal receptor function. Examination of the macroscopic kinetics associated with GABA-evoked currents allowed us to further uncover the impact each mutation has on receptor function. We characterized the receptor kinetics of macroscopic deactivation following a brief (3 ms) pulse of saturating GABA, similar to that occurring during synaptic transmission (Fig. 4). When the deactivation time constants were extracted by fitting bi-exponential functions it was observed that both single mutations significantly accelerated deactivation (wild-type: $\tau_w = 37.4 \pm 5.5 \text{ ms}$; D163A: $\tau_w = 15.6 \pm 1.2 \text{ ms}$; R120A: $\tau_w = 3.5 \pm 0.2 \text{ ms}$). Also, the double mutant has the same deactivation time constant as R120A (R120A/D163A: $\tau_w = 3.5 \pm 0.3 \text{ ms}$).

MOL #68619

Double-mutant cycle analysis of the deactivation time constant revealed a significant coupling energy of 0.5 kcal/mol (Table 2). This coupling energy suggests that the contributions of β_2 D163 and α_1 R120 to the function of deactivation are not independent, and that they interact during this phase. Deactivation has a very complex nature and is comprised of numerous microscopic parameters, any of which could be functionally coupled for β_2 D163 and α_1 R120. Changes in the deactivation phase are often associated with changes in the microscopic unbinding rate, but other transitions such as desensitization and channel closing can influence deactivation (Jones and Westbrook, 1995). In order to investigate which of these microscopic transitions are responsible for the coupling found in the deactivation time constants of β_2 D163 and α_1 R120, we performed kinetic modeling as presented in a later section.

R120A suppresses desensitization

Further assessment of macroscopic data was conducted to explore the functional effect of D163A and R120A, as well as to provide additional constraint for kinetic modeling. Macroscopic desensitization was characterized during a long (500ms) pulse of saturating GABA and the resulting desensitization phase was fit with a bi-exponential function from which a weighted time constant was calculated (Fig. 5). Unlike D163A, which had little effect on desensitization, R120A and R120A/D163A show a visible reduction of desensitization in raw traces (Fig. 5A). Comparison of the weighted τ values revealed R120A and R120A/D163A have significantly slower desensitization (wild-type: $\tau_w = 124 \pm 10$ ms; D163A: $\tau_w = 85 \pm 6$ ms; R120A: $\tau_w = 218 \pm 23$ ms; R120A/D163A: $\tau_w = 242 \pm 33$ ms) (Fig. 5B). The extent of desensitization displayed by R120A and R120A/D163A is similarly reduced, unlike that of D163A, which remains normal (wild-type: 61 ± 2 %; D163A: 66 ± 2 %; R120A: 53 ± 2 %; R120A/D163A: 39 ± 3 %) (Fig. 5C).

MOL #68619

Microscopic unbinding rates are strongly coupled for D163A and R120A

In order to determine the microscopic basis for the coupling of deactivation effects caused by D163A and R120A we employed a previously established 7-state kinetic model (Fig. 6A) (Jones and Westbrook, 1995; Wagner et al., 2004; Barberis et al., 2007; Goldschen-Ohm et al., 2010). This is a simplified model that recapitulates the dominant features present in our macroscopic $\alpha\beta\gamma$ receptor data. It incorporates several known features of GABA_A receptor physiology including two binding steps (Bormann and Clapham, 1985), multiple open states (Macdonald et al., 1989), and desensitized states that can occur prior to opening (Burkat et al., 2001). We also utilized an unlinked unbinding step, as was required by Goldschen-Ohm et al. (2010), which was necessary to consistently simulate our experimental data.

Prior to model optimization we performed nonstationary variance analysis (Supplemental Fig. 2) (Sigworth, 1980). This assessment provides a measure of both the single-channel conductance and maximal open probability (P_{o-max}) of each receptor type, which can be used to further constrain our modeling. None of the mutations altered conductance (γ) at -60 mV or the P_{o-max} (wild-type: $\gamma = 32 \pm 3$ pS, $P_{o-max} = 0.59 \pm 0.05$; D163A: $\gamma = 33 \pm 3$ pS, $P_{o-max} = 0.55 \pm 0.03$; R120A: $\gamma = 29 \pm 3$ pS, $P_{o-max} = 0.58 \pm 0.06$; R120A/D163A: $\gamma = 31 \pm 3$ pS, $P_{o-max} = 0.57 \pm 0.04$). We simultaneously fit current responses to 3 ms and 500 ms pulses of saturating GABA for each receptor type. Initially k_{on} and P_{o-max} were fixed to their experimentally determined rates and the remaining parameters were set at the values previously reported by Goldschen-Ohm et al. (2010). The model was then optimized under relatively tight constraints until values for the opening and closing rates (α_1 , β_1 , α_2 , β_2), as well as for entry into D1, were obtained that gave

MOL #68619

consistently good fits to our data. These values were identical for all constructs except for the opening rate of the dominant open state (β_2), which varied for each mutant to account for the slower rise times observed for the mutant constructs during responses to saturating concentrations of GABA (Supplemental Fig. 3). With these values constrained, a second optimization run was performed in which only the unbinding rates (k_{off}) and the rates for entering and leaving the doubly-bound desensitized state (D2) were allowed to vary. Our model quantitatively reproduced both wild-type and mutant data (Fig. 6B and C). The models for all three of our mutant constructs display slower binding and faster unbinding of GABA relative to wild type. The models for R120A and R120A/D163A also have slower entry and a more rapid exit from the doubly-bound desensitized state (D2). When double-mutant cycle analysis is applied to the modeled unbinding rates, coupling energies of 0.63 kcal/mol and 0.34 kcal/mol were calculated for k_{off1} and k_{off2} , respectively (Table 2). This indicates that coupled effects on unbinding are the basis for the coupling seen in deactivation.

MOL #68619

Discussion

In order to build upon our understanding of the structure of the GABA binding site and the functional significance of specific residues, we experimentally tested for the existence of an interaction across the β/α interface between β_2 D163 and α_1 R120. It has been demonstrated that mutating either residue alters the GABA concentration-response curve, but whether either of these residues is involved in binding, gating, or desensitization has been speculative. Here the residues were mutated to alanine and double-mutant cycle analysis was applied to a variety of macroscopic and microscopic parameters. Intriguingly, the residues appear to be completely independent when considering the binding of GABA, but they are coupled when looking at the unbinding of GABA. These results suggest that β_2 D163 and α_1 R120 do not interact in the unbound state but form an interaction upon binding of GABA.

Evidence for a salt-bridge between β_2 D163 and α_1 R120

The effects on unbinding (k_{off}) for β_2 D163A and α_1 R120A were coupled with an energy of 0.63 kcal/mol. This energy is slightly lower than, but consistent with energies reported for confirmed surface salt-bridges in other proteins (0.86 kcal/mol and 0.95 kcal/mol) (Horovitz et al., 1990; Makhatdze et al., 2003). Low coupling energies are expected because salt-bridges at solvent-exposed surfaces of a protein have significantly weaker interactions compared to those buried in the hydrophobic interior. In the case of β_2 D163 and α_1 R120, both are exposed to the aqueous environment, as demonstrated by SCAM studies (Kloda and Czajkowski, 2007; Newell et al., 2004). Additionally, the strength of a salt-bridge is influenced by the distance between the two residues. In homology models of the GABA_A receptor, the nearest charged groups of β_2 D163 and α_1 R120 are 3.6 angstroms apart (O'Mara et al., 2005), just within range for a salt-bridge.

MOL #68619

Because the coupling energy between pairs of residues decreases with distance, the weaker coupling energy measured in our experiments may be the consequence of this distance.

Therefore, we believe the coupling energy observed with β_2 D163A and α_1 R120A represents the loss of a salt-bridge.

It is also important to acknowledge additional interpretations to a significant coupling energy. A predicted interaction may not exclusively be direct, but could result from secondary interactions through a third side chain, or could be the result of indirect coupling due to broader structural rearrangements or conformational changes. Although we cannot rule out such possibilities, the presumed proximity of these residues suggests a direct interaction.

A state-dependent interaction

Transient salt-bridges may provide a mechanism for governing conformational changes and stabilization of specific receptor states. In this study, double-mutant cycle analysis reveals that an interaction between β_2 D163 and α_1 R120 occurs during unbinding, but not binding steps **indicating that an interaction between these two residues stabilizes the bound-closed states (B1 and B2 on our model)**. A state-dependent interaction is not difficult to envision, where these residues are coupled during the GABA bound state, but not during the unbound state. In the unbound receptor no interaction is present; when GABA binds, conformational changes occur that move the residues into position to interact. Conformational rearrangements in response to GABA binding are expected and repeatedly observed in studies of the binding pocket (Wagner and Czajkowski, 2001; Newell et al., 2004; Muroi et al., 2006). In fact, β_2 D163 itself, along with other residues on loop B of the β_2 subunit, has been shown to undergo rearrangements

MOL #68619

in response to receptor activation (Newell et al., 2004). This movement may underlie the state-dependence of the interaction between β_2 D163 and α_1 R120. State-dependent electrostatic interactions for residues coupled to the open state of nicotinic acetylcholine receptors have also been proposed (Kash et al., 2003; Gleitsman et al., 2008). Additionally, there is growing evidence in the field of protein structure supporting the occurrence of salt-bridge switching, especially where networks of charged residues are involved (Law and Lightstone, 2009).

Aspartic acid and arginine are capable of forming multiple electrostatic interactions. Aspartic acid has two partial negative charges distributed between the two oxygen atoms of the carboxylic group; and arginine has three nitrogens in its guanidinium group. Therefore, it is likely that **β_2 D163 and α_1 R120 participate in a larger ionic network. While no specific additional interactions for β_2 D163 and α_1 R120 have been identified, a number of polar side chains are found in close proximity. Candidates for participation in this extended ionic network include, but are not limited to α_1 N88, β_2 R28, β_2 D95, and nearby backbone amides and carbonyls (Fig. 7A). α_1 N88 is just one example of numerous polar residues located nearby that could also participate in an ionic network. The homology model based on the AChBP actually shows β_2 R28 participating in a ternary ionic network with β_2 D163 and α_1 R120 (Cromer et al., 2002).**

β_2 D95, located on loop A and proximal to α_1 R120, is particularly intriguing. The equivalent residues in the glycine receptor (α_1 D97 and α_1 R119) participate in a state-dependent inter-subunit electrostatic interaction (Todorovic et al., 2010). This interaction is proposed to exist when the glycine receptor is in the unbound state and is broken upon

MOL #68619

the binding of agonist. This result from the glycine receptor, argues for a model in which α_1 R120 of the GABA receptor interacts with β_2 D95 (on loop A) in the unbound state and is handed off to β_2 D163 (on loop B) upon binding of agonist.

Discontinuity in functional effects

β_2 D163 and α_1 R120 appear to interact in the ligand-bound state; however, the residues have asymmetric roles in desensitization. α_1 R120A displays greatly reduced desensitization, while β_2 D163A displays desensitization indistinguishable from wild type. We propose that these residues, as part of a dynamic region, can stabilize the bound-closed receptor without necessarily influencing the rate-limiting transitions of desensitization. The additional effect observed for α_1 R120A may be the byproduct of its involvement in a complex electrostatic network. It is highly probable that a simple binary interaction is not occurring between β_2 D163 and α_1 R120. Several examples of an arginine residue simultaneously making multiple interactions have been identified (Horovitz et al., 1990; Borders et al., 1994). The multifaceted functional group of α_1 R120 may be participating in an additional interaction that is separate from β_2 D163 and is critical to desensitization transitions. Under these circumstances, an interaction between β_2 D163 and α_1 R120 could exist in all bound receptor states, and still yield asymmetric effects when either is mutated.

Functional role of β_2 D163- α_1 R120 interaction

The interaction between β_2 D163 and α_1 R120 appears to be highly conserved, not just at the β/α interface where a negative and a positive residue are found at these positions on every isoform of β and α subunits, but also at other inter-subunit interfaces (**Fig. 7B**). Recently, a corresponding

MOL #68619

interaction at the γ/β interface was identified (Goldschen-Ohm et al., 2010). This interaction consisted of a triad of charge residues (β_2 R117, γ_2 E178, and γ_2 R43) forming a salt-bridge network. The additional arginine (γ_2 R43) is conserved at the β/α interface (β_2 R28), but was not investigated in our current study. This conserved motif may play an important role in establishing the architecture at each subunit interface.

Goldschen-Ohm et al. (2010) reported that mutation at any of the residues in this motif slowed deactivation following a GABA response. Not only is this significant because it demonstrates that a homologous interaction influences ligand binding at other subunit interfaces, but it is also significant because disruption of this interaction at the γ/β interface had the opposite effect of disruption of the corresponding interaction at the β/α interface. Mutation of either β_2 D163 or α_1 R120 significantly increases the rate of deactivation. We propose this inter-subunit motif is involved in subunit positioning. In this scenario, breaking of the interaction at the β/α interface may increase the distance between the β and α subunits, speeding unbinding, whereas breaking the interaction at the γ/β interface may reduce the distance between the β and α subunits at the β/α interface, slowing unbinding.

The GABA binding site is involved in desensitization

This study is the first to offer in depth characterization of α_1 R120. We provide results that demonstrate α_1 R120 has important roles in GABA binding/unbinding and desensitization. It should not be lost in this discussion that α_1 R120 is the first residue at the GABA binding pocket that shows a dramatic influence in desensitization (particularly the early, fast phase). Most work regarding desensitization has focused on the transmembrane domains, and previous studies have

MOL #68619

demonstrated a significant role for the pre-M1 region in transducing desensitization to the pore surrounded by the TM2 domain (Bianchi and Macdonald, 2002). The identification of α_1 R120 may provide a unique focus for studying how desensitization is transduced from the GABA binding site.

MOL #68619

Acknowledgements

We thank Marcel Goldschen-Ohm for assistance with data analysis.

MOL #68619

Authorship Contributions

Participated in research design: Laha and Wagner.

Conducted experiments: Laha.

Performed data analysis: Laha and Wagner.

Wrote or contributed to the writing of the manuscript: Laha and Wagner.

Other: Wagner acquired funding for the research.

MOL #68619

References

Barberis A, Mozrzymas JW, Ortinski PI and Vicini S (2007) Desensitization and binding properties determine distinct $\alpha 1\beta 2\gamma 2$ and $\alpha 3\beta 2\gamma 2$ GABA(A) receptor-channel kinetic behavior. *Eur J Neurosci* **25**:2726-2740.

Baumann SW, Baur R and Sigel E (2002) Forced subunit assembly in $\alpha 1\beta 2\gamma 2$ GABAA receptors. Insight into the absolute arrangement. *J Biol Chem* **277**:46020-46025.

Benke D, Fritschy JM, Trzeciak A, Bannwarth W and Mohler H (1994) Distribution, prevalence, and drug binding profile of gamma-aminobutyric acid type A receptor subtypes differing in the beta-subunit variant. *J Biol Chem* **269**:27100-27107.

Bianchi MT and Macdonald RL (2002) Slow phases of GABA(A) receptor desensitization: structural determinants and possible relevance for synaptic function. *J Physiol (Lond)* **544**:3-18.

Bollan K, King D, Robertson LA, Brown K, Taylor PM, Moss SJ and Connolly CN (2003) GABA(A) receptor composition is determined by distinct assembly signals within alpha and beta subunits. *J Biol Chem* **278**:4747-4755.

Borders CL, Jr, Broadwater JA, Bekeny PA, Salmon JE, Lee AS, Eldridge AM and Pett VB (1994) A structural role for arginine in proteins: multiple hydrogen bonds to backbone carbonyl oxygens. *Protein Sci* **3**:541-548.

Bormann J and Clapham DE (1985) gamma-Aminobutyric acid receptor channels in adrenal chromaffin cells: a patch-clamp study. *Proc Natl Acad Sci USA* **82**:2168-2172.

MOL #68619

Brejč K, van Dijk WJ, Klaassen RV, Schuurmans M, van Der Oost J, Smit AB and Sixma TK (2001) Crystal structure of an ACh-binding protein reveals the ligand-binding domain of nicotinic receptors. *Nature* **411**:269-276.

Burkat PM, Yang J and Gingrich KJ (2001) Dominant gating governing transient GABA(A) receptor activity: a first latency and Po/o analysis. *J Neurosci* **21**:7026-7036.

Colquhoun D (1998) Binding, gating, affinity and efficacy: the interpretation of structure-activity relationships for agonists and of the effects of mutating receptors. *Br J Pharmacol* **125**:924-947.

Colquhoun D and Hawkes AG (1995a) The principles of the stochastic interpretation of ion-channel mechanisms. in *Single-channel recording* (B. Sakmann and E. Neher eds) pp 397-482, Plenum, New York.

Colquhoun D and Hawkes AG (1995b) A Q-matrix cookbook. How to write only one program to calculate the single-channel and macroscopic predictions for any kinetic mechanism. in *Single-channel recording* (B. Sakmann and E. Neher eds) pp 589-633, Plenum, New York.

Cromer BA, Morton CJ and Parker MW (2002) Anxiety over GABA(A) receptor structure relieved by AChBP. *Trends Biochem Sci* **27**:280-287.

Gleitsman KR, Kedrowski SM, Lester HA and Dougherty DA (2008) An intersubunit hydrogen bond in the nicotinic acetylcholine receptor that contributes to channel gating. *J Biol Chem* **283**:35638-35643.

MOL #68619

Goldschen-Ohm MP, Wagner DA, Petrou S and Jones MV (2010) An epilepsy-related region in the GABA(A) receptor mediates long-distance effects on GABA and benzodiazepine binding sites. *Mol Pharmacol* **77**:35-45.

Horovitz A (1996) Double-mutant cycles: a powerful tool for analyzing protein structure and function. *Fold Des* **1**:R121-6.

Horovitz A, Serrano L, Avron B, Bycroft M and Fersht AR (1990) Strength and co-operativity of contributions of surface salt bridges to protein stability. *J Mol Biol* **216**:1031-1044.

Jones MV, Jonas P, Sahara Y and Westbrook GL (2001) Microscopic kinetics and energetics distinguish GABA(A) receptor agonists from antagonists. *Biophys J* **81**:2660-2670.

Jones MV, Sahara Y, Dzubay JA and Westbrook GL (1998) Defining affinity with the GABAA receptor. *J Neurosci* **18**:8590-8604.

Jones MV and Westbrook GL (1995) Desensitized states prolong GABA_A channel responses to brief agonist pulses. *Neuron* **15**:181-191.

Kash TL, Jenkins A, Kelley JC, Trudell JR and Harrison NL (2003) Coupling of agonist binding to channel gating in the GABA(A) receptor. *Nature* **421**:272-275.

Kash TL, Trudell JR and Harrison NL (2004) Structural elements involved in activation of the gamma-aminobutyric acid type A (GABAA) receptor. *Biochem Soc Trans* **32**:540-546.

MOL #68619

Kloda JH and Czajkowski C (2007) Agonist-, antagonist-, and benzodiazepine-induced structural changes in the alpha1 Met113-Leu132 region of the GABAA receptor. *Mol Pharmacol* **71**:483-493.

Law RJ and Lightstone FC (2009) Modeling neuronal nicotinic and GABA receptors: important interface salt-links and protein dynamics. *Biophys J* **97**:1586-1594.

Macdonald RL, Rogers CJ and Twyman RE (1989) Kinetic properties of the GABA_A receptor main conductance state of mouse spinal neurones in culture. *J Physiol (Lond)* **410**:479-499.

Makhatadze GI, Loladze VV, Ermolenko DN, Chen X and Thomas ST (2003) Contribution of surface salt bridges to protein stability: guidelines for protein engineering. *J Mol Biol* **327**:1135-1148.

McKernan RM and Whiting PJ (1996) Which GABAA-receptor subtypes really occur in the brain? *Trends Neurosci* **19**:139-143.

Muroi Y, Czajkowski C and Jackson MB (2006) Local and global ligand-induced changes in the structure of the GABA(A) receptor. *Biochemistry* **45**:7013-7022.

Newell JG, McDevitt RA and Czajkowski C (2004) Mutation of glutamate 155 of the GABAA receptor beta2 subunit produces a spontaneously open channel: a trigger for channel activation. *J Neurosci* **24**:11226-11235.

O'Mara M, Cromer B, Parker M and Chung SH (2005) Homology model of the GABAA receptor examined using Brownian dynamics. *Biophys J* **88**:3286-3299.

MOL #68619

Padgett CL, Hanek AP, Lester HA, Dougherty DA and Lummis SC (2007) Unnatural amino acid mutagenesis of the GABA(A) receptor binding site residues reveals a novel cation-pi interaction between GABA and beta 2Tyr97. *J Neurosci* **27**:886-892.

Price KL, Millen KS and Lummis SC (2007) Transducing agonist binding to channel gating involves different interactions in 5-HT3 and GABAC receptors. *J Biol Chem* **282**:25623-25630.

Sigworth FJ (1980) The variance of sodium current fluctuations at the node of Ranvier. *J Physiol (Lond)* **307**:97-129.

Taylor PM, Thomas P, Gorrie GH, Connolly CN, Smart TG and Moss SJ (1999) Identification of amino acid residues within GABA(A) receptor beta subunits that mediate both homomeric and heteromeric receptor expression. *J Neurosci* **19**:6360-6371.

Todorovic J, Welsh BT, Bertaccini EJ, Trudell JR, and Mihic SJ (2010) Disruption of an intersubunit electrostatic bond is a critical step in glycine receptor activation. *Proc Natl Acad Sci USA* **107**:7987-7992.

Wagner DA and Czajkowski C (2001) Structure and dynamics of the GABA binding pocket: A narrowing cleft that constricts during activation. *J Neurosci* **21**:67-74.

Wagner DA, Czajkowski C and Jones MV (2004) An arginine involved in GABA binding and unbinding but not gating of the GABA(A) receptor. *J Neurosci* **24**:2733-2741.

Westh-Hansen SE, Witt MR, Dekermendjian K, Liljefors T, Rasmussen PB and Nielsen M (1999) Arginine residue 120 of the human GABAA receptor alpha 1, subunit is essential for GABA binding and chloride ion current gating. *Neuroreport* **10**:2417-2421.

MOL #68619

Footnotes

This research was supported by the National Institutes of Health [Grant NS055793].

Address correspondence to: Kurt T. Laha, Department of Biological Sciences, Marquette University, P.O. Box 1881, Milwaukee, Wisconsin 53201-1881, USA. Email:

kurt.laha@marquette.edu

MOL #68619

Figure Legends

Figure 1. Homology models of the GABA_A receptor depict a putative salt-bridge between β_2 D163 and α_1 R120. A) Side view of the extracellular domain at a single β/α interface. The nearest charged atoms of α_1 R120 and β_2 D163 are 3.6 Å apart. B) Sequences of various human GABA_A receptor, glycine receptor, 5-HT_{3A} receptor, and nicotinic acetylcholine receptor subunits aligned with the acetylcholine binding protein sequence, demonstrates the conservation of the residues mutated in this study.

Figure 2. Mutant cycle analysis of EC_{50-GABA} indicates α_1 R120 and β_2 D163 are weakly coupled. A) GABA concentration-response curves for single and double alanine mutations at α_1 R120 and β_2 D163 when measuring peak GABA responses. B) The mutant cycle for these alanine mutations. Equations for calculating the change in free energy associated with each mutation and the overall coupling energy are listed in the methods.

Figure 3. GABA binds more slowly to R120A, D163A, and R120A/D163A. A) Race experiments of either single alanine mutation or the double alanine mutation of α_1 R120 and β_2 D163. For wild-type and D163A receptors, currents evoked by simultaneous application of 3 mM GABA and 300 μ M SR-95531 (gray traces) were compared with the current evoked by 3 mM GABA alone (black traces). For R120A and R120A/D163A receptors, currents evoked by simultaneous application of 30 mM GABA and 300 μ M SR-95531 (gray traces) were compared with the current evoked by 30 mM GABA alone (black traces). The two separate applications are overlaid for each receptor type, and the ratio of the peak currents is indicated with an arrow.

Figure 4. Deactivation is faster for R120A, D163A, and R120A/D163A. A) Macroscopic current responses to a 3 ms pulse of saturating GABA (indicated by arrow). Each mutant

MOL #68619

response is overlaid with the normalized wild-type response (light gray). B) Summary of weighted time constants (τ_w) for deactivation, generated from bi-exponential fits of the macroscopic currents. τ_w is computed as $\sum a_i \cdot \tau_i / \sum a_i$ where a_i and τ_i are the amplitude and time constant of component i .

Figure 5. Macroscopic desensitization during a long GABA pulse. A) Macroscopic current responses to a 500 ms pulse of saturating GABA (indicated by black bar above trace). Each mutant response is overlaid with the normalized wild-type response (light gray). (B and C) Macroscopic currents for all receptor types were fit with a bi-exponential equation, although several responses for R120A and R120A/D163A only required a mono-exponential during fits. B) Summary of weighted time constants for desensitization. C) Summary of the extent of desensitization after 500 ms.

Figure 6. Kinetic modeling demonstrates that the effects of R120A, D163A, and R120A/D163A can be similarly explained by faster unbinding rates, while differential changes in desensitization occur. A) The 7-state markov model used to simulate GABA responses (U, unbound; B, bound; O, open; D, desensitized). B) Rate constants used to simultaneously simulate responses to short and long pulses of saturating GABA for wild-type, D163A, R120A, and R120A/D163A. The units are s^{-1} except for GABA binding steps, which are $M^{-1} \cdot s^{-1}$. Only k_{off1} , k_{off2} , r_1 , d_2 , r_2 , and p are reported as \pm standard error because they were allowed to vary while the model was optimized. C) Current responses (black trace) and simulated responses (red trace) to both short pulse and long pulses of GABA are displayed for each receptor type.

Figure 7. Possible inter-subunit ionic networks exist in homology models of the GABA_A receptor. A) Side view of the extracellular domain at a single β/α interface. Polar side-chains in

MOL #68619

the vicinity of β_2 D163 and α_1 R120, which may contribute to the ionic network, are depicted. B)
View from the extracellular side looking through the channel pore. β_2 D163 and α_1 R120 are
located at the β/α inter-subunit interfaces and are also conserved at the other interfaces.

MOL #68619

Table 1. Summary of microscopic binding and unbinding rates and macroscopic affinity for the competitive antagonist SR-95531

	K_{D-SR}	k_{off-SR}	k_{on-SR}
Wild-type	140 nM	$15.9 \pm 0.8 \text{ s}^{-1}$	$1.2 \pm 0.1 \times 10^8 \text{ M}^{-1}\text{s}^{-1}$
D163A	110 nM	$10.3 \pm 0.7 \text{ s}^{-1} *$	$9.7 \pm 0.6 \times 10^7 \text{ M}^{-1}\text{s}^{-1}$
R120A	100 nM	$11.5 \pm 0.4 \text{ s}^{-1} *$	$1.2 \pm 0.1 \times 10^8 \text{ M}^{-1}\text{s}^{-1}$
R120A/D163A	100 nM	$11.1 \pm 0.9 \text{ s}^{-1} *$	$1.2 \pm 0.1 \times 10^8 \text{ M}^{-1}\text{s}^{-1}$

Significant differences between control and mutant parameters were calculated using ANOVA with a Dunnett's post-test (* $p < 0.05$)

MOL #68619

Table 2. Summary of macroscopic and microscopic parameters used for double-mutant cycle analysis

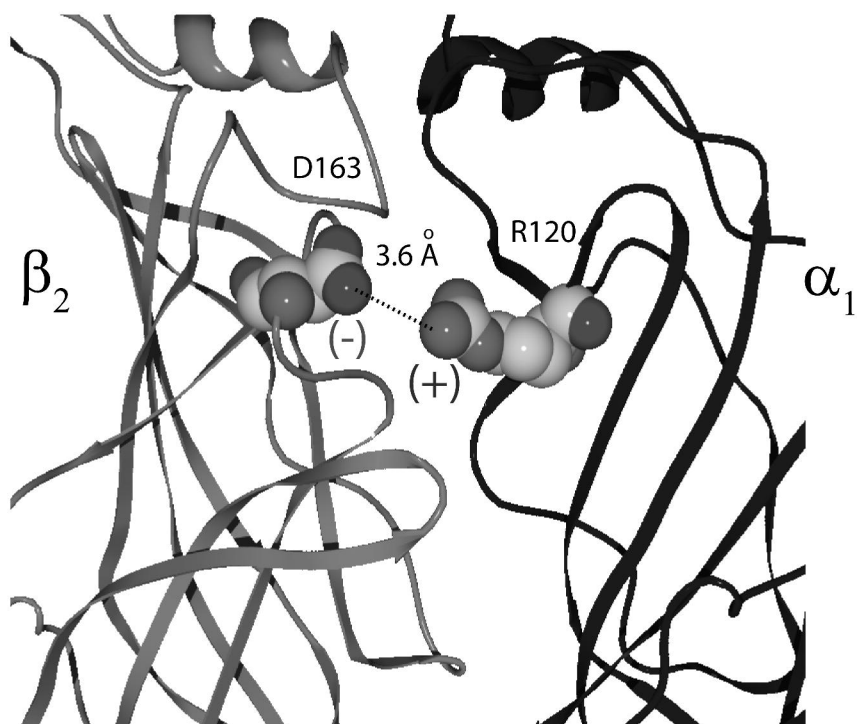
	Wild-type	D163A	R120A	R120A/D163A	$ \Delta\Delta G_{\text{coupling}} $
$EC_{50\text{-GABA}}$	65 μM	155 μM	920 μM	1600 μM	0.2 kcal/mol
Deactivation τ_w	37.4 ms	15.6 ms *	3.5 ms *	3.5 ms *	0.5 kcal/mol
k_{on}	$7.4 \times 10^6 \text{ M}^{-1}\text{s}^{-1}$	$4.3 \times 10^6 \text{ M}^{-1}\text{s}^{-1}$ *	$8.3 \times 10^5 \text{ M}^{-1}\text{s}^{-1}$ *	$5.0 \times 10^5 \text{ M}^{-1}\text{s}^{-1}$ *	0.03 kcal/mol
k_{off1}	8 s^{-1} *	21 s^{-1} *	118 s^{-1} *	108 s^{-1} *	0.63 kcal/mol
k_{off2}	271 s^{-1} *	485 s^{-1} *	1072 s^{-1} *	1079 s^{-1} *	0.34 kcal/mol

Significant differences between control and mutant parameters were calculated using ANOVA

with a Dunnett's post-test (* $p < 0.05$)

Figure 1

A.



B.

Loop E

Loop B

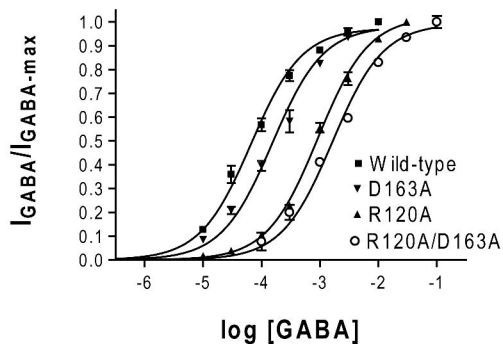
R120
*

D163
*

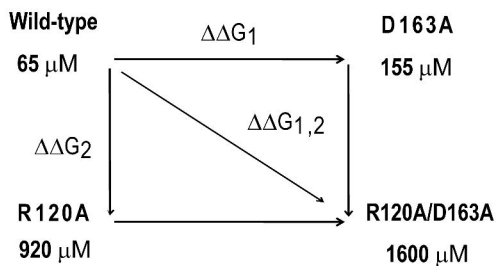
GABA α_1	..NKLL R ITEDGTLTYMR..	..CTLEFGSYAYTRA E VVYE..
GABA β_2	..NRMI R LHPDGTVLYGLR..	..CPLKIESYGYTTD D IEFY..
GABA γ_2	..NRML R IWNDGRVLYSLR..	..CPLEFSSYGYPRE E IVYQ..
GABA ρ_1	..NVML R VQPDGKVLVSLR..	..CSLEIESYAYTED D LMLY..
GlyR α_1	..NKLL R ISRNGNVLYSIR..	..CIMQLESFGYTMN D LIFE..
5-HT3A	..YVYI R H..QGEVQNYKP..	..CSLTFTSWLHTIQ D INIS..
nAChR α_1	..MTKLLD D YTGKIMWTPP..	..CTMKLGIWTYDGT K VSIS..
AChBP	..PQLA R VVSDGEVLYMPS..	..CRIKIGSWTHHSR E ISVD..

Figure 2

A.



B.



$$\Delta\Delta G_1 = 0.5 \text{ kcal/mol}$$

$$\Delta\Delta G_2 = 1.6 \text{ kcal/mol}$$

$$\Delta\Delta G_{1,2} = 1.9 \text{ kcal/mol}$$

$$\Delta\Delta G_{\text{coupling}} = -0.2 \text{ kcal/mol}$$

Figure 3

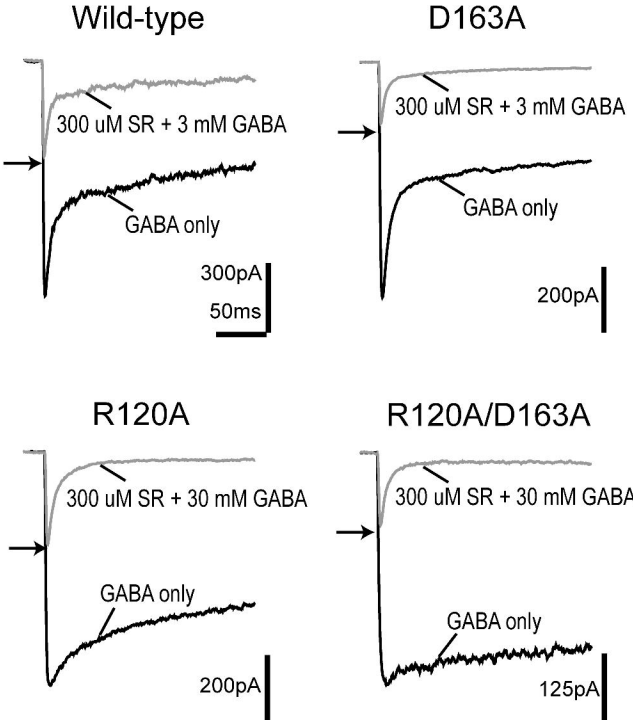
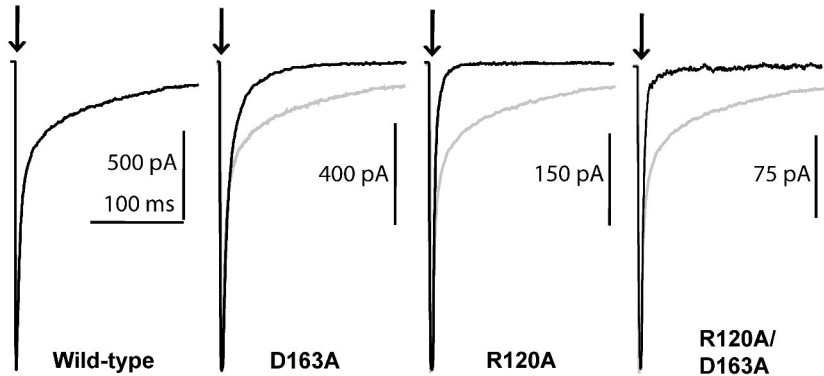


Figure 4

A.

GABA



B.

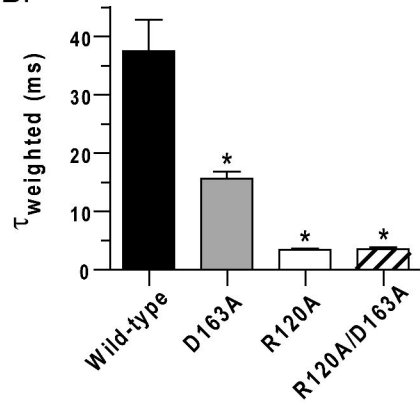
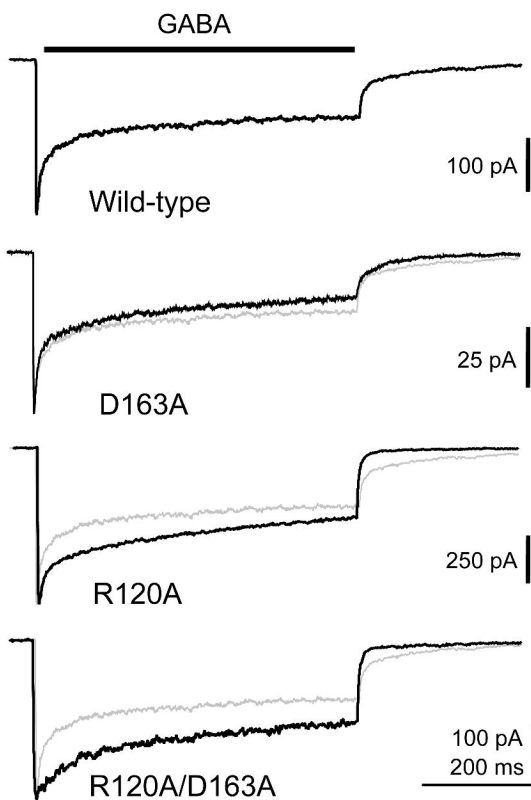
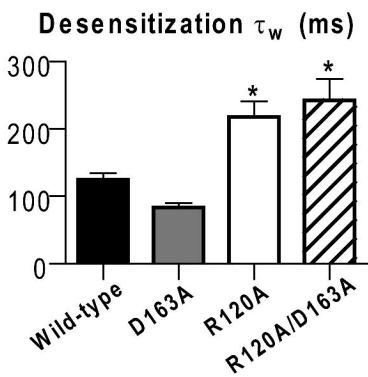


Figure 5

A.



B.



C.

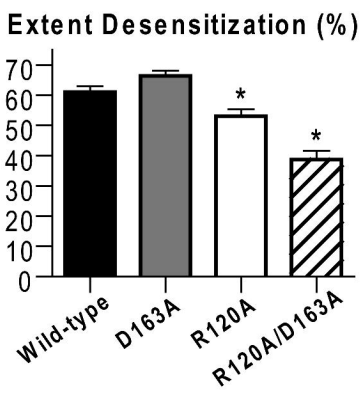
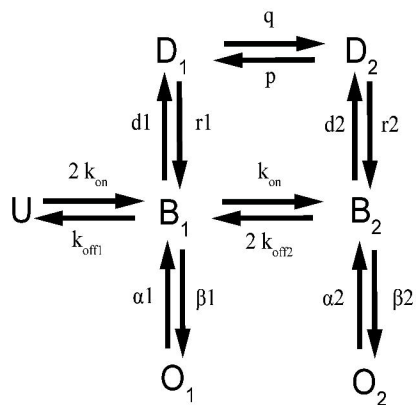


Figure 6

A.



B.

	Wild-type	D163A	R120A	R120A/D163A
k_{on}	7.4×10^6	4.3×10^6	8.3×10^5	5.0×10^5
k_{off1}	8 ± 2	$21 \pm 5^*$	$118 \pm 7^*$	$108 \pm 10^*$
k_{off2}	271 ± 45	$485 \pm 35^*$	$1072 \pm 26^*$	$1079 \pm 18^*$
β_1	400	400	400	400
α_1	2800	2800	2800	2800
β_2	2500	2250	2000	1750
α_2	1000	1000	1000	1000
d_1	12	12	12	12
r_1	3.2 ± 0.3	3.3 ± 0.3	4.8 ± 2.2	2.4 ± 0.3
d_2	371 ± 38	390 ± 16	$75 \pm 8^*$	$60 \pm 18^*$
r_2	115 ± 6	106 ± 6	$89 \pm 8^*$	$49 \pm 14^*$
q	0.03	0.03	0.03	0.03
p	5.7 ± 0.4	5.8 ± 0.7	5.7 ± 0.5	4.9 ± 0.8

C.

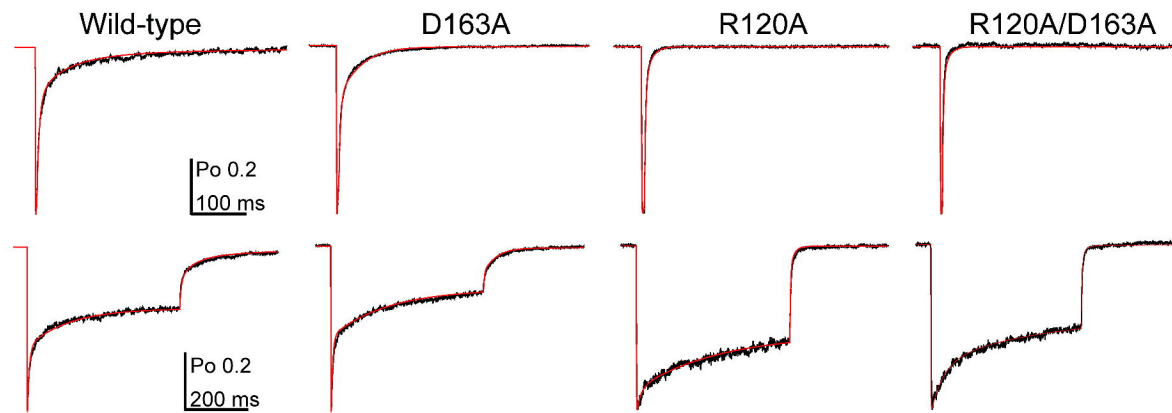
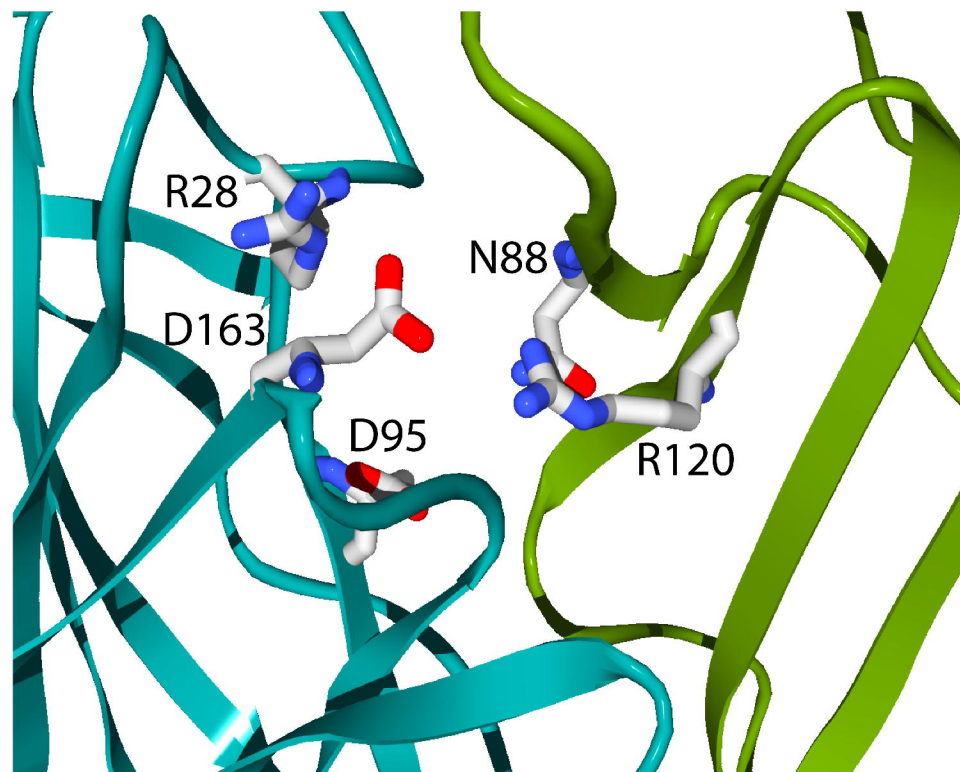


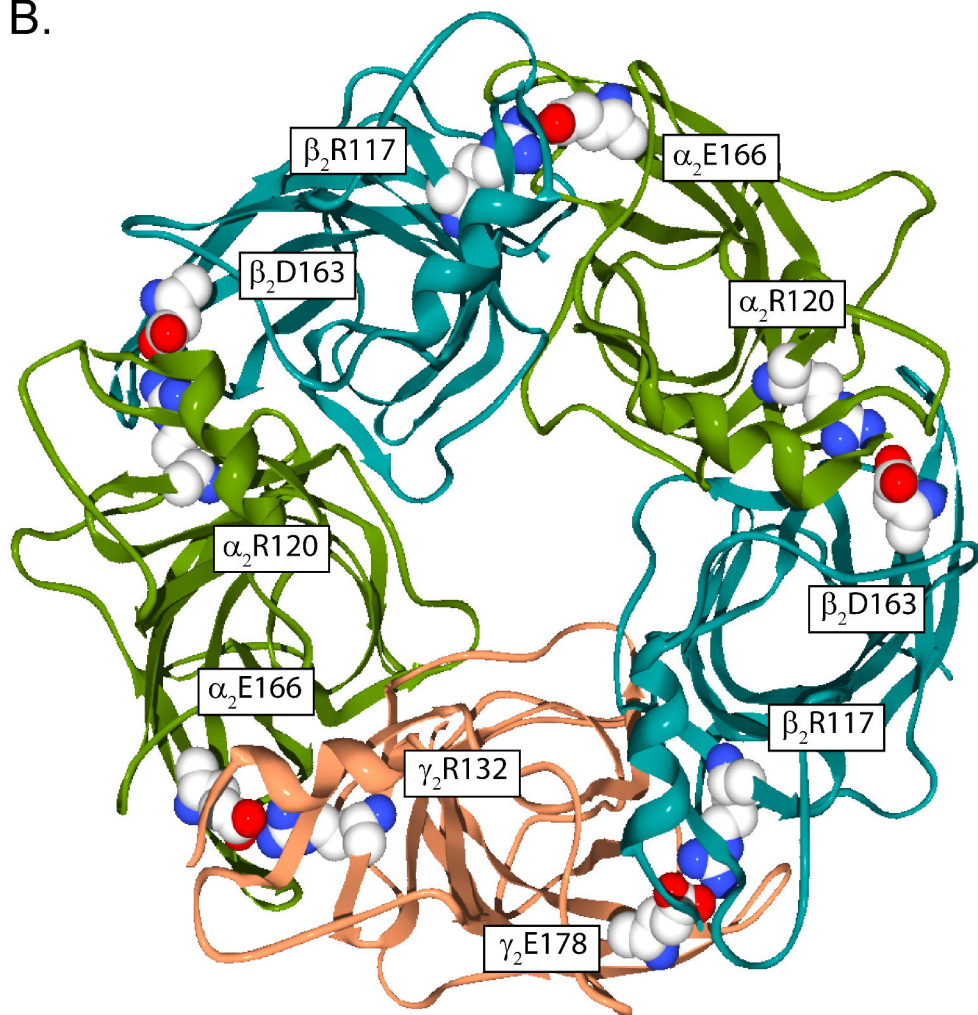
Figure 7

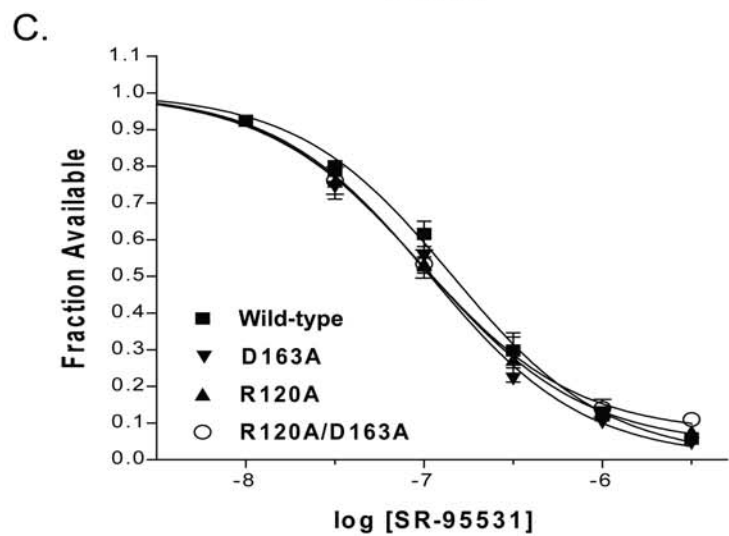
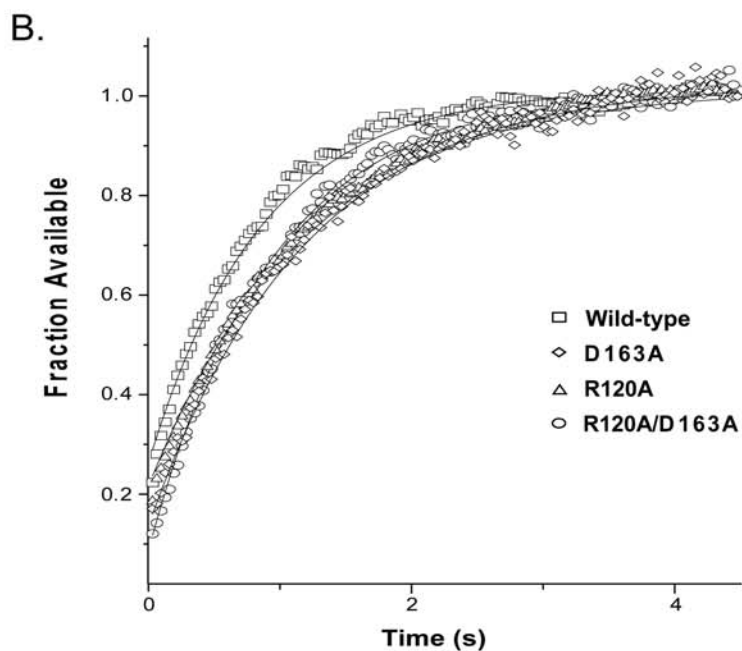
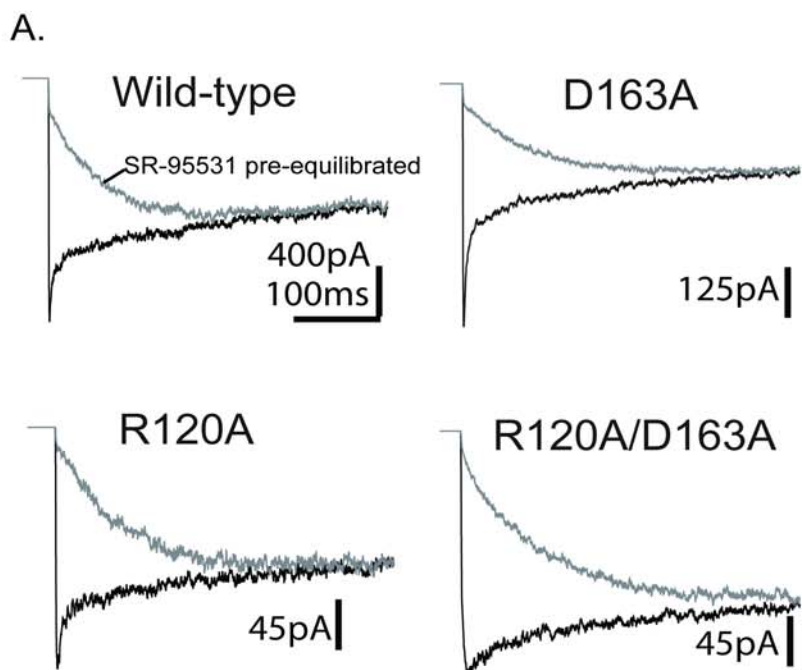
This article has not been copyedited and formatted. The final version may differ from this version.

A.

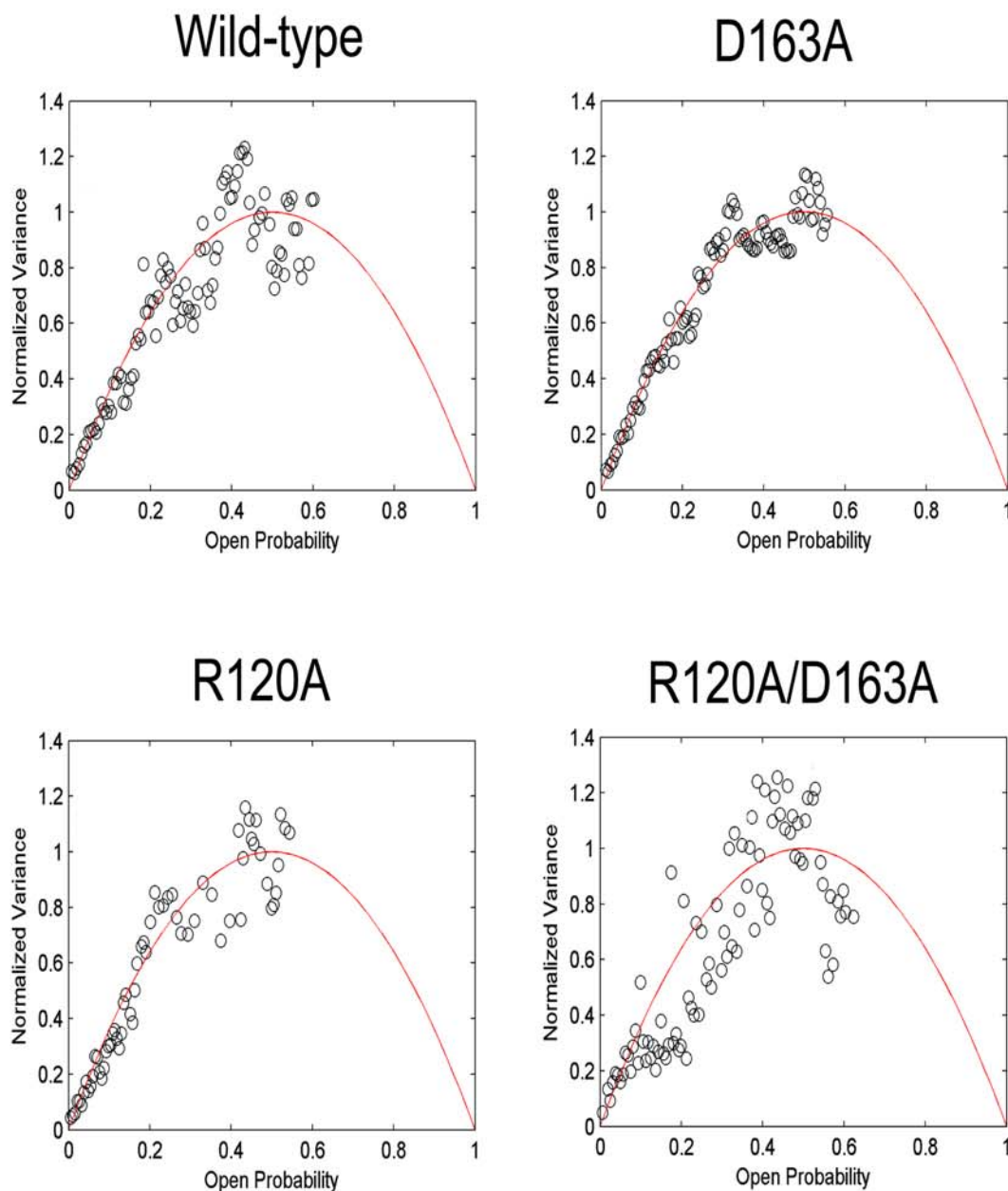


B.

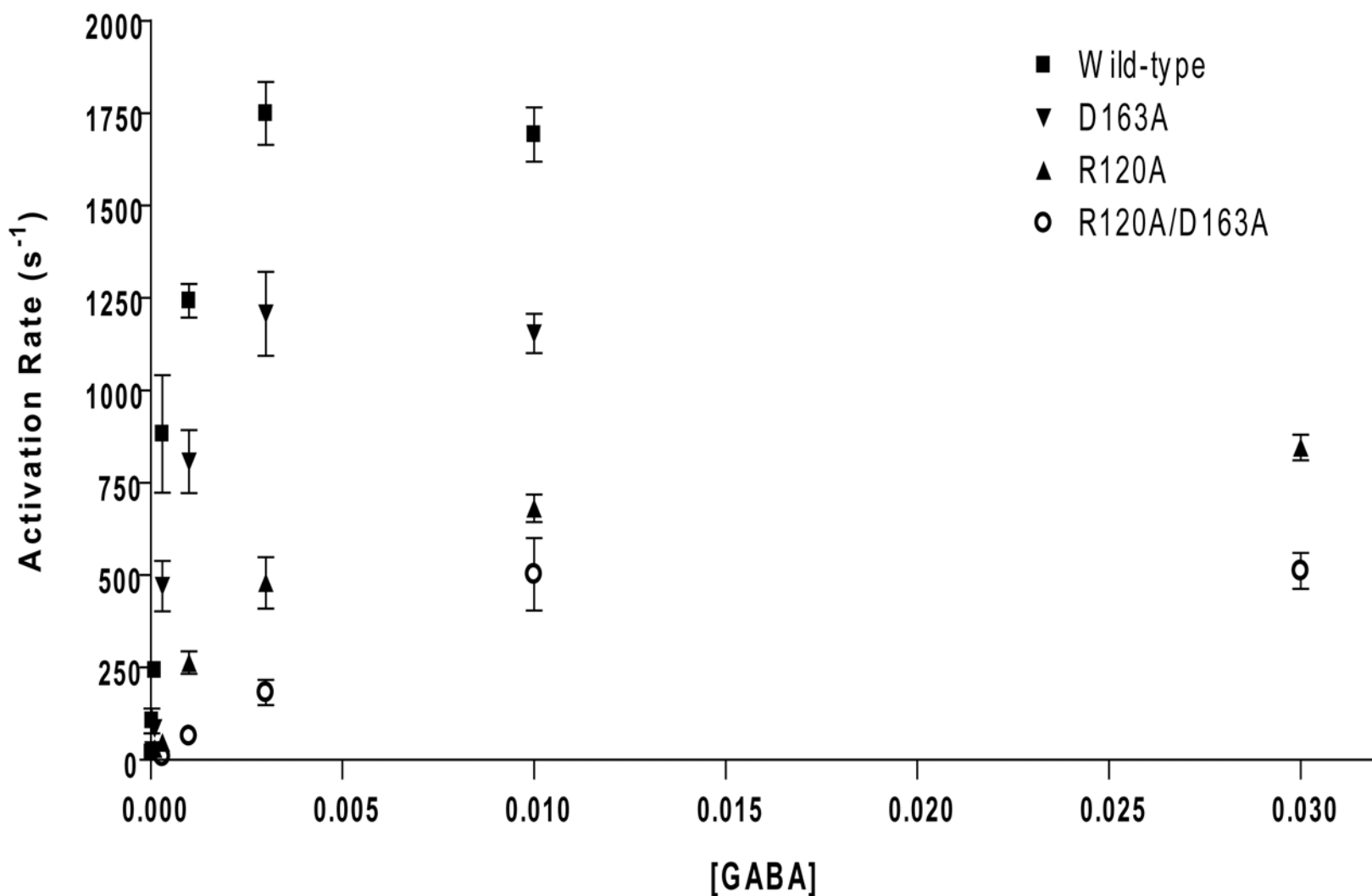




Supplemental Figure 1. Microscopic kinetics for the antagonist SR-95531. A) The K_D , k_{off} , and k_{on} for SR-95531 was determined for each receptor type by examining the current response to 30 mM GABA following a pre-incubation in a series of concentrations of SR-95531 (1 μ M shown above). B) Deconvolution of GABA-evoked currents after SR-95531 pre-equilibration from control currents (no pre-equilibration) reveals the time course of SR-95531 unbinding. Deconvolved traces were fit to the equation $A(t) = [P_\infty - (P_\infty - P_0)\exp(t/\tau_u)]^N$, where $A(t)$ is the fraction of available receptors (antagonist not bound at any site), P_0 and P_∞ are the probabilities that a single binding site is available initially at $t=0$ and at steady state as $t \rightarrow \infty$, τ_u is the time constant of antagonist unbinding from each site ($k_{off-SR} = 1/\tau_u$), and N is the number of binding sites (Jones et al., 2001). C) Dose response curves for the equilibrium antagonist occupancy in the absence of GABA $A(t=0)$ were fit to the normalized hill equation $I/I_{max} = 1 - 1/[(K_{D-SR}/[SR-95531])^N + 1]$.



Supplemental Figure 2. Nonstationary variance analysis demonstrates that these mutations do not affect the peak open probability (P_{o-max}). Plots are of normalized mean current versus variance for each receptor type. Data points were fit with a parabola describing the single channel conductance, P_{o-max} , and the number of channels present in each patch, none of which differed between constructs (Student's t-test).



Supplemental Figure 3. The rise times during activation of GABA responses were measured from 10-90% (baseline to peak). The activation rates (1/rise time) are plotted against GABA concentration for each receptor type demonstrating that the rising rates saturate for each of the constructs (wild-type 10 mM GABA: 1562 ± 98 s⁻¹; D163A 10 mM GABA: 1075 ± 58 s⁻¹; R120A 30 mM GABA: 813 ± 33 s⁻¹; R120A/D163A 30 mM GABA: 498 ± 40 s⁻¹). Mutant cycle analysis of the rise rates yields a coupling energy of -0.07 kcal/mol and indicates R120A and D163A have independent effects on rise rates.